Available online at www.sciencedirect.com
SCIENCE DIRECT®
International Journal of Heat and Mass Transfer 49 (2006) 4672–4680
International Journal of HEAT and MASS TRANSFER
www.elsevier.com/locate/ijhmt

Thermal lattice-BGK model based on large-eddy simulation of turbulent natural convection due to internal heat generation ☆

Hongjuan Liu, Chun Zou *, Baochang Shi, Zhiwei Tian, Liqi Zhang, Chuguang Zheng

State Key Laboratory of Coal Combustion, Huazhong University of Science and Technology, Wuhan 430074, People's Republic of China

Received 30 June 2005; received in revised form 30 March 2006
Available online 14 June 2006

Abstract

To simulate turbulent convection at high Rayleigh number (*Ra*), we propose a new thermal lattice-BGK (LBGK) model based on large eddy simulation (LES). Two-dimensional numerical simulations of natural convection with internal heat generation in a square cavity were performed at *Ra* from 10^6 to 10^{13} with Prandtl numbers (*Pr*) at 0.25 and 0.60. Simulation results indicate that our model is fit to simulate high *Ra* flow for its better numerical stability. At $Ra = 10^{13}$, a global turbulent has occurred. With a further increase in *Ra*, the flow will arrive in a fully turbulence regime. The Nusselt–Rayleigh relationship is also discussed.

Keywords: Thermal LBGK model; LES; Turbulent convection; High *Ra*

1. Introduction

Turbulent thermal convection is ubiquitous [1] in nature and technology, and serves important and diverse purposes. Natural convection (NC) flows due to internal heat generations has been lately receiving increase attention because of its relevance to nuclear safety issues. While the Rayleigh–Bénard convection (RBC) has been extensively studied, the literature on NC driven by internal heat is confined to fewer studies (see Ref. [2], for a list of references).

Turbulent convection sets in at high *Ra* [1,3–5]. However, it is still a challenge for both experiments and numerical simulations to capture the turbulent flow motion at high *Ra*. In fact, the highest *Ra* attainable in an apparatus of a given size is usually quite limited for a fluid such as water. Because of the unknown properties of the core melt at high temperatures, the researchers were unable to reproduce adequate accident conditions. Moreover, it is not a simple task to measure *Pr* dependence in convection turbulence by experiments. Therefore, numerical simulations are required to predict the turbulent flows especially at very high *Ra*.

For the smallest scales in the turbulent flows at high *Ra* are of the same magnitude with the Kolmogorov microscales, flows turbulence modeling becomes necessary. A viable alternative to the direct numerical simulation (DNS) is the method of LES [3,6], a time-honored method in engineering fluid mechanics and meteorology, which may be the only way to simulate the time-dependent physics in its full complexity while keeping a reasonable accuracy at the largest scales. Horvat et al. [2,7] simulated the NC flow with internal heat generation in a square cavity for a wide range of *Ra* and *Pr*: *Ra* 10^6–10^{13} and *Pr* 0.25–8 by using LES.

Since the NC flows at high *Ra* have complex behavior, efficient methods are still needed for further studies, especially for 3D problems. The LBGK method is a candidate for such methods [8,9]. For non-isothermal flows, several

☆ The work is supported by the State Key Development Programmer for Basic Research of China under Grant Nos. 2004CB217700.
* Corresponding author. Tel.: +86 27 87542417 8314.
E-mail address: zouchun@mail.hust.edu.cn (C. Zou).

0017-9310/$ - see front matter © 2006 Elsevier Ltd. All rights reserved.
doi:10.1016/j.ijheatmasstransfer.2006.03.038

Nomenclature

c	particle speed
C	Smagorinsky constant
D	thermal diffusivity
D_t	turbulent thermal diffusivity
$\vec{e}_i$	discrete velocity
f_i, T_i	force term in Eqs. (2) and (5)
g	gravity
g_i, θ_i	distribution function for velocity and temperature field
g_i^{eq}, θ_i^{eq}	equilibrium distribution function for velocity and temperature field
L	length of simulation domain
I	volumetric heat generation
Nu	Nusselt number
Nu_{up}	Nusselt number for upper surface
p	pressure
Pr	Prandtl number ($=\nu/D$)
Pr_t	turbulent Prandtl number
Ra	Rayleigh number ($=g\beta IL^3/\nu D$)
S_{ij}	strain rate tensor
T	simulation time interval
$\vec{u}$	fluid velocity vector
$\vec{x}$	phase space

Greek symbols

β	temperature dilatation
ϵ	Knudsen number
θ	dimensionless temperature
ν	kinematic viscosity
ν_t	turbulent eddy viscosity
τ	relaxation time
$\tau_{\vec{u}}$, $\tau_{\vec{\theta}}$	relaxation time for velocity and temperature field
$\omega = \tau^{-1}$	relaxation parameter
ω_i	the weights for equilibrium distribution function
Δ	filter width
Δt	time step
Δx, Δy	grid spacing in x- and y-directions

Subscripts and superscripts

α, β	spatial index
i	discrete velocity direction
total	total index
0	initial index
$-$	filter operator

temperature LBGK (TLBGK) models have been developed [10–12]. However, most of these models suffer from complicated evolution equations [12] or severe numerical instability [13]. Recently, Guo et al. [14] propose a new TLBGK model with a robust boundary scheme. Although the model holds if viscous heating effects and compression work are negligible [15] and the boundary conditions simulate only imposed temperature [16], it has proved to have good stability as well as simplicity. Using the model, Shi [17] had succeeded in simulating the NC flows due to internal heat generation in a square cavity at Ra 10^6–10^{12} and Pr 0.25 and 0.60. However, the LBGK method is still viewed as a DNS so that it is limited to resolve relatively low Ra flows. For example, when $Ra = 10^{12}$ and $Pr = 0.25$, the simulation with the TLBGK model results in numerical instability. To extend the LBGK method to turbulent flows, it is natural to incorporate the existing turbulent models into the framework of the LBGK method. There are some paradigms which succeed in combining LES with the LBGK model to simulate isotherm flows at high Re [18–20]. Inspired by this idea, we propose a new TLBGK model based on LES which directly introduce the Smagorinsky eddy viscosity [6] to the TLBGK model. The approach will be presented in the second part of the paper.

To understand heat transfer at high Ra, the relationship between the Nusselt number (Nu) and Ra has drawn much attention as a scaling law [21–23]. However, the issue of the existence of an asymptotic regime that is supposed to occur at very high Ra remains an open one. Theory [21] predicted that a full turbulent regime arises in such a state $Nu = Ra^{\beta}$ with $\beta = 1/2$. But large amounts of convection experiments [4,22] revealed that some other exponents β such as 2/7 or 1/3 existed. Moreover, a recent theoretical study [23] has suggested that the $Nu(Ra)$ relation should not follow a strict power-law. As to the NC of internally heated fluids, a considerable amount of experimental and analysis effort was focused on determining the averaged Nu numbers on the cooled surface in many geometries such as fluid layer, rectangular, semicircular and elliptical cavities. Although the geometries were different, the relationship $Nu_{up}(Ra)$ for the upper surfaces are quite similar [24]. Hence, the question arises of whether or not a simple power-law relationship between Nu and Ra exists in turbulent natural convection due to internal heat generation. Since the fluid used in the above mentioned literatures were mostly water ($Pr = 2.5$–7) and Freon ($Pr = 8$–11), to answer the question, large numbers of numerical simulations at a large range Ra with relative low Pr are needed to be performed.

In the paper, we simulate natural convection flows due to internal heat generation in a cavity for Ra up to 10^{13} with Pr at 0.25 and 0.60 using the TLBGK model based on LES. Simulation results with isotherms and the time-boundary-averaged Nu vs. Ra figures are presented in the third part of the paper. Meanwhile, the relationship $Nu(Ra)$ is discussed. In the last part, conclusions are drawn based on these simulation results.

2. The numerical algorithm

2.1. The TLBGK model [14]

The fluid in the present work is governed by 2D time-dependent Navier–Stokes equations using Boussinesq approximation to include buoyancy forces, and the dimensionless forms read [17]

$$\nabla \cdot \vec{u} = 0 \tag{1a}$$

$$\frac{\partial \vec{u}}{\partial t} + \vec{u} \cdot \nabla \vec{u} = -\nabla p + v\Delta \vec{u} + Pr\Theta \frac{\vec{g}}{|\vec{g}|} \tag{1b}$$

$$\frac{\partial \Theta}{\partial t} + \vec{u} \cdot \nabla \Theta = D\Delta\Theta + D \tag{1c}$$

A complete description of the scaling procedure may be found in Ref. [25]. The boundary conditions are taken to be $\vec{u} = 0$ and $\Theta = 0$ on all the four walls; the initial conditions are set to be $\vec{u} = 0$; $\Theta = 0$ for all cases.

Based on the idea of the TLBGK model [14], we add a force term $f_i (= \frac{Pr}{2c}\alpha_i \vec{e}_i \cdot \frac{\vec{g}}{|\vec{g}|}\Theta)$ to the evolution equation for the velocity field to recover the force term in Eq. (1b) (see Appendix A for details):

$$g_i(\vec{x} + c\vec{e}_i\Delta t, t + \Delta t) - g_i(\vec{x}, t) = -\frac{1}{\tau_{\vec{u}}}(g_i(\vec{x}, t) - g_i^{\mathrm{eq}}(p, \vec{u})) + \Delta t f_i \tag{2}$$

where $\alpha_i = \delta_{i2} + \delta_{i4}$ and $i = 0, 1, \ldots, 8$. The particle speed $c = \Delta x/\Delta t$, Δx and Δt are the lattice grid spacing and the time step, respectively. $g_i(\vec{x}, t)$ is the distribution function and $\tau_{\vec{u}}$ is the relaxation time for the velocity field. The discrete velocities $\vec{e}_i$ of the $d2q9$ LBGK model [25] are defined as

$$\vec{e}_i = \begin{cases} (0,0), & i = 0 \\ (\cos(i-1)\pi/2, \sin(i-1)\pi/2), & i = 1,2,3,4 \\ \sqrt{2}(\cos(i-5)\pi/2 + \pi/4, \sin(i-5)\pi/2 + \pi/4), & i = 5,6,7,8 \end{cases}$$

For the values of the parameters appeared in the equilibrium distribution function g_i^{eq} of the TLBGK model [14] are replaced by $\sigma = 5/12$, $\lambda = 1/3$, $\gamma = 1/12$, g_i^{eq} can be simplified as

$$g_i^{\mathrm{eq}} = \begin{cases} -\dfrac{5p}{3c^2} + s_i(\vec{u}), & i = 0 \\ \dfrac{p}{3c^2} + s_i(\vec{u}), & i = 1,2,3,4 \\ \dfrac{p}{12c^2} + s_i(\vec{u}), & i = 5,6,7,8 \end{cases} \tag{3}$$

where $s_i(\vec{u}) = \omega_i\left[3\dfrac{\vec{e}_i \cdot \vec{u}}{c} + 4.5\dfrac{(\vec{e}_i \cdot \vec{u})^2}{c^2} - 1.5\dfrac{|\vec{u}|^2}{c^2}\right]$, $\omega_0 = 4/9$, $\omega_i = 1/9$ $(i = 1,2,3,4)$ and $\omega_i = 1/36$ $(i = 5,6,7,8)$.

The flow velocity, pressure and kinetic viscosity are given by

$$\vec{u} = \sum_{i=1}^{8} c\vec{e}_i g_i, \quad p = \frac{3c^2}{5}\left(\sum_{i=1}^{8} g_i - \frac{2|\vec{u}|^2}{3c^2}\right),$$

$$v = \frac{c^2}{3}\left(\tau_{\vec{u}} - \frac{1}{2}\right)\Delta t \tag{4}$$

Similarly, we utilize an LBGK equation with $d2q5$ lattice [27] for Eq. (1c)

$$\Theta_i(\vec{x} + c\vec{e}_i\Delta t, t + \Delta t) - \Theta_i(\vec{x}, t) = -\frac{1}{\tau_\Theta}(\Theta_i(\vec{x}, t) - \Theta_i^{\mathrm{eq}}(p, \vec{u})) + \Delta t T_i \quad (i = 0,1,2,3,4) \tag{5}$$

where $\Theta_i(\vec{x}, t)$ is the distribution function and τ_Θ is the relaxation time for the temperature field, $\Theta_i^{\mathrm{eq}} = \frac{\Theta}{5}(1 + 2.5\frac{\vec{e}_i \cdot \vec{u}}{c})$, and $T_i = \frac{D}{5}(1 + 2.5\frac{\vec{e}_i \cdot \vec{u}}{c})$. The temperature and the thermal diffusivity are calculated by

$$\Theta = \sum_{i=0}^{4} \Theta_i, \quad D = \frac{2c^2}{5}\left(\tau_\Theta - \frac{1}{2}\right)\Delta t \tag{6}$$

It should be noted that the other lattices could also be used for Eq. (5), say $d2q4$ in Ref. [14]. It was found that the TLBGK with $d2q5$ has better numerical stability than that with $d2q4$ for the flows considered here.

For the boundary schemes, the non-equilibrium extrapolation method for the velocity and pressure boundary conditions [14,17] are used.

2.2. The LES Smagorinsky model [2]

As to the turbulent convection at high Ra, the subgrid scale effect of turbulence on the resolved flow field is calculated by eddy viscosity v_t and turbulent thermal diffusivity $D_t = (v_t/Pr_t)$, where Pr_t is the turbulent Prandtl number. So that the LES Smagorinsky model was implemented, with modification to capture the buoyancy forces due to the temperature gradients. Thus,

$$v_t = (C\Delta)^2\left(|\overline{S}|^2 + \frac{Pr}{Pr_t}\nabla\Theta \cdot \frac{\vec{g}}{|\vec{g}|}\right)^{1/2} \tag{7}$$

The first term in Eq. (7) represents stress forces while the second term represents buoyancy. The constant C is called the Smagorinsky constant and is adjustable. In our case, we take $C(=0.1)$ which is the same as in Ref. [2], whereas Pr_t is set to 0.4. And $\Delta = \sqrt{(\Delta x)^2 + (\Delta y)^2}$ is the filter width, Δx and Δy are the grid spacings in the x- and y-directions. $|\overline{S}| = \sqrt{2\overline{S}_{\alpha\beta}\overline{S}_{\alpha\beta}}$ is the magnitude of the large scale strain rate tensor with $\overline{S}_{\alpha\beta} = (\partial_\alpha \bar{u}_\beta + \partial_\beta \bar{u}_\alpha)/2$, where the over bar indicates filtered values.

2.3. The TLBGK based model on LES

It is easy to implement the LES Smagorinsky model into the LBGK model [18–20]. Following the idea of LES, we assume that the collision steps in the LBGK model only correlate with some local information and the forms of the filtered equilibrium distribution are all the same as in Eq. (3), except now we will use the filtered quantities to replace the unfiltered quantities. In addition, considering

the local eddy viscosity effect, we will incorporate the Smagorinsky eddy viscosity ν_t into the relaxation time $\tau_{\vec{u}}$.

Since the spatial dependence of the relaxation time $\tau_{\vec{u}}$ will not change the Chapman–Enskog expansion procedure [26] and does not affect the derivation of the Navier–Stokes equations, using the equation for kinetic viscosity in Eq. (4), we still have

$$\nu_{\text{total}} = \frac{c^2}{3}\left(\tau_{\vec{u}} - \frac{1}{2}\right)\Delta t = \nu_0 + \nu_t \tag{8}$$

where ν_{total} is the total viscosity, ν_0 is the initial kinetic viscosity. Assumed $\tau_0 = \frac{3\nu_0}{c^2\Delta t} + \frac{1}{2}$, from Eq. (8) we can get

$$\tau_{\vec{u}} = \frac{3\nu_{\text{total}}}{c^2\Delta t} + \frac{1}{2} = \frac{3(\nu_0+\nu_t)}{c^2\Delta t} + \frac{1}{2} = \frac{3\nu_0}{c^2\Delta t} + \frac{1}{2} + \frac{3\nu_t}{c^2\Delta t} = \tau_0 + \frac{3\nu_t}{c^2\Delta t} \tag{9}$$

Next we will explain how to obtain ν_t based on the LBGK model. Assumed $Q = \sum_{i=0}^{8} e_{i\alpha}e_{i\beta}(\bar{g}_i - \bar{g}_i^{\text{eq}})$, then (see Appendix A for details)

$$|\overline{S}| = \frac{3}{2\tau_{\vec{u}}\Delta t}|Q| \tag{10}$$

Substituting Eq. (10) to Eq. (7) for the modified Smagorinsky eddy viscosity ν_t, then

$$\nu_t = (C\Delta)^2\left(\frac{9}{4\tau_{\vec{u}}^2\Delta t^2}|Q|^2 + \frac{Pr}{Pr_t}\nabla\Theta\cdot\frac{\vec{g}}{|\vec{g}|}\right)^{1/2} \tag{11}$$

Eq. (9) can be changed to

$$\tau_{\text{total}} = \tau_0 + \frac{3(C\Delta)^2}{c^2\Delta t}\left(\frac{9}{4\tau_{\vec{u}}^2\Delta t^2}|Q|^2 + \frac{Pr}{Pr_t}\nabla\Theta\cdot\frac{\vec{g}}{|\vec{g}|}\right)^{1/2} \tag{12}$$

As for the isothermal turbulent flow ($\nabla\Theta = 0$), from the above equation, we can get

$$\tau_{\vec{u}} = \frac{\tau_0 + \sqrt{\tau_0 + 18C^2|Q|}}{2} \tag{13}$$

However, Eq. (12) is generally difficult to solve. In our numerical simulations, for simplicity, the values of $\tau_{\vec{u}}$ in the right hand of Eq. (12) are just substituted by those in the preceding time step. Then we can directly obtain $\tau_{\vec{u}}$ for the current moment from Eq. (12).

For the temperature field, the thermal diffusivity D in Eq. (6) is replaced by D_{total}, which still satisfies

$$D_{\text{total}} = \frac{2c^2}{5}\left(\tau_\Theta - \frac{1}{2}\right)\Delta t \tag{14}$$

By analogy with Eq. (9), we can obtain

$$\tau_\Theta = \tau_{\Theta 0} + \frac{2.5D_t}{c^2\Delta t} = \tau_{\Theta 0} + \frac{2.5\nu_t/Pr_t}{c^2\Delta t} \tag{15}$$

where $\tau_{\Theta 0} = \frac{2.5D_0}{c^2\Delta t} + \frac{1}{2}$. And then the value of τ_Θ in Eq. (5) can be renewed.

It is obviously that the only change to the previous TLBGK model happens on the relaxation time, $\tau_{\vec{u}}$ and τ_Θ. For the renewed relaxation time has become the function both of space and time, the TLBGK model based on LES is no longer a model with single-time-relaxation approximation which accords with the characteristics of turbulence of the highly locality.

3. Numerical results and discussion

Using the TLBGK model based on LES, we simulate natural convection in the square cavity due to internal heat generation for Ra 10^6–10^{13} with Pr of 0.25 and 0.6 for all cases. The lattice size is 256×256 for Ra from 10^6 to 10^{12}. But only in the case of 10^{13}, we use a 512×512 grid to improve the resolution. The initial relaxation parameter $\omega_0 = \tau_0^{-1}$ is set to be the same as in Ref. [17]. Generally, the LBGK method will become unsteady when $\omega_0 \to 2$ which limit it to simulate relatively low Reynolds flow. In Ref. [17], the TLBGK model is helpless when $Ra > 10^{12}(\omega > 1.991)$ because of the numerical instability. As for our TLBGK model based on LES, the simulation results have proved it to keep stable even when $\omega_0 = 1.998$. Considering the physical signification as well as the numerical stability, the TLBGK model based on LES is more fit for high Ra flow.

3.1. Isotherms for Ra 10^6–10^{13}

Fig. 1 presents snapshots of the temperature field for different combinations of Ra and Pr at the end of the dimensionless simulation time T.

From Fig. 1(a) and (b) we can see that for $Ra = 10^6$ and $Ra = 10^7$, steady-state conditions are both reached at the end of the simulations, and the horizontal symmetries are preserved.

In Fig. 1(c) we show the temperature fields for $Ra = 10^8$ obtained at time $T = 0.1$ after 10^5 time steps. The symmetry of the fluid circulation is broken, and steady-state conditions are not reached at the end of the simulation. The turbulence first appears at the side and upper boundaries, whereas the fluid flow in the lower region of the simulation domain stays symmetrical.

In Fig. 2(a) for $Ra = 10^9$ (at $T = 0.05$), the flow structure becomes more complicated. The Rayleigh–Taylor instabilities at the upper and Kelvin–Hemholtz instabilities at the side boundaries extend the local instabilities to the whole domain. At the same time, the heat transfer at the bottom becomes intense, especially in the lower corner of the simulation domain. Although the symmetry is broken at such Rayleigh numbers, the flow is still a transition to turbulence. When $Ra = 10^9$, the effect of Pr becomes distinct. From Fig. 2(a) we can see, the influence of the thermal on the upper wall for $Pr = 0.60$ is intense but local, whereas the influence is more global for $Pr = 0.25$. However the heat transfer on the bottom shows even more instability for $Pr = 0.25$.

In Fig. 2(b) for $Ra = 10^{11}$ (at $T = 0.015$), heat transfer on the boundaries of the simulation domain exhibits large random-like peaks, and some small localized patches have

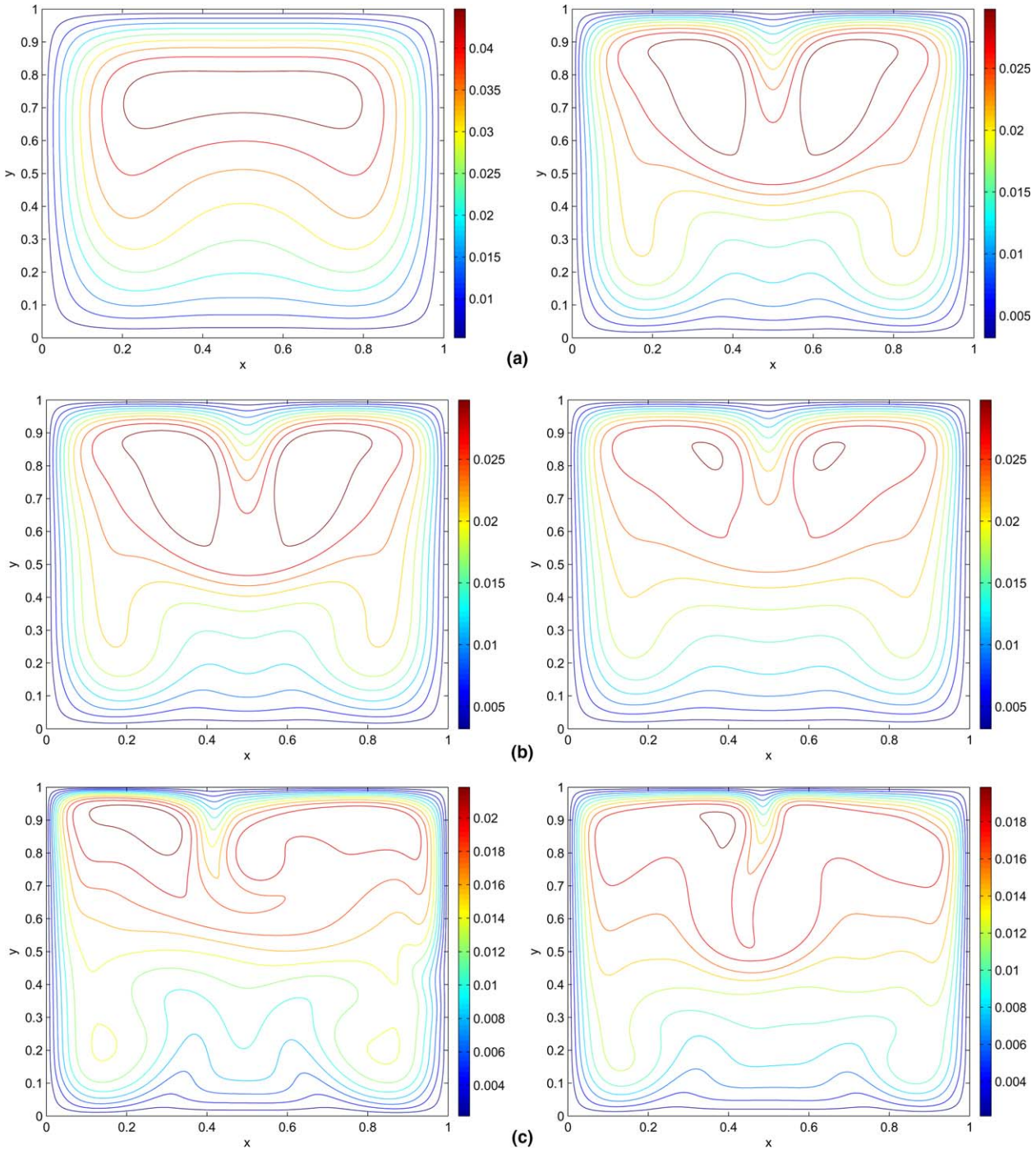

Fig. 1. Isotherms: $Pr = 0.25$ (left) and $Pr = 0.60$ (right). (a) $Ra = 10^6$, (b) $Ra = 10^7$, (c) $Ra = 10^8$.

occurred in the vicinity of the boundaries. However, in the middle of the simulation domain, the large-scale flow structures still dominate.

When the Ra is increased to 10^{13} (Fig. 2(c)), the entire simulation domain becomes irregular and chaotic. The small-scale structures become increasing and much finer. Filaments and patches of thermal anomalies distribute everywhere which are the characteristics of turbulence. It can be concluded that with a further increase of Ra, the flow becomes even more turbulent. The flow structures of $Pr = 0.60$ resemble those of $Pr = 0.25$ which indicate Pr does not significantly influence the time to reach the turbulent conditions.

3.2. Time-boundary-averaged Nusselt numbers

To quantify the results, the time-boundary-averaged Nusselt numbers [2] obtained by our TLBGK model based on LES are plotted in Fig. 3, including those in Refs. [2,17]. It can be found that our results for $Ra \leqslant 10^9$ agree well

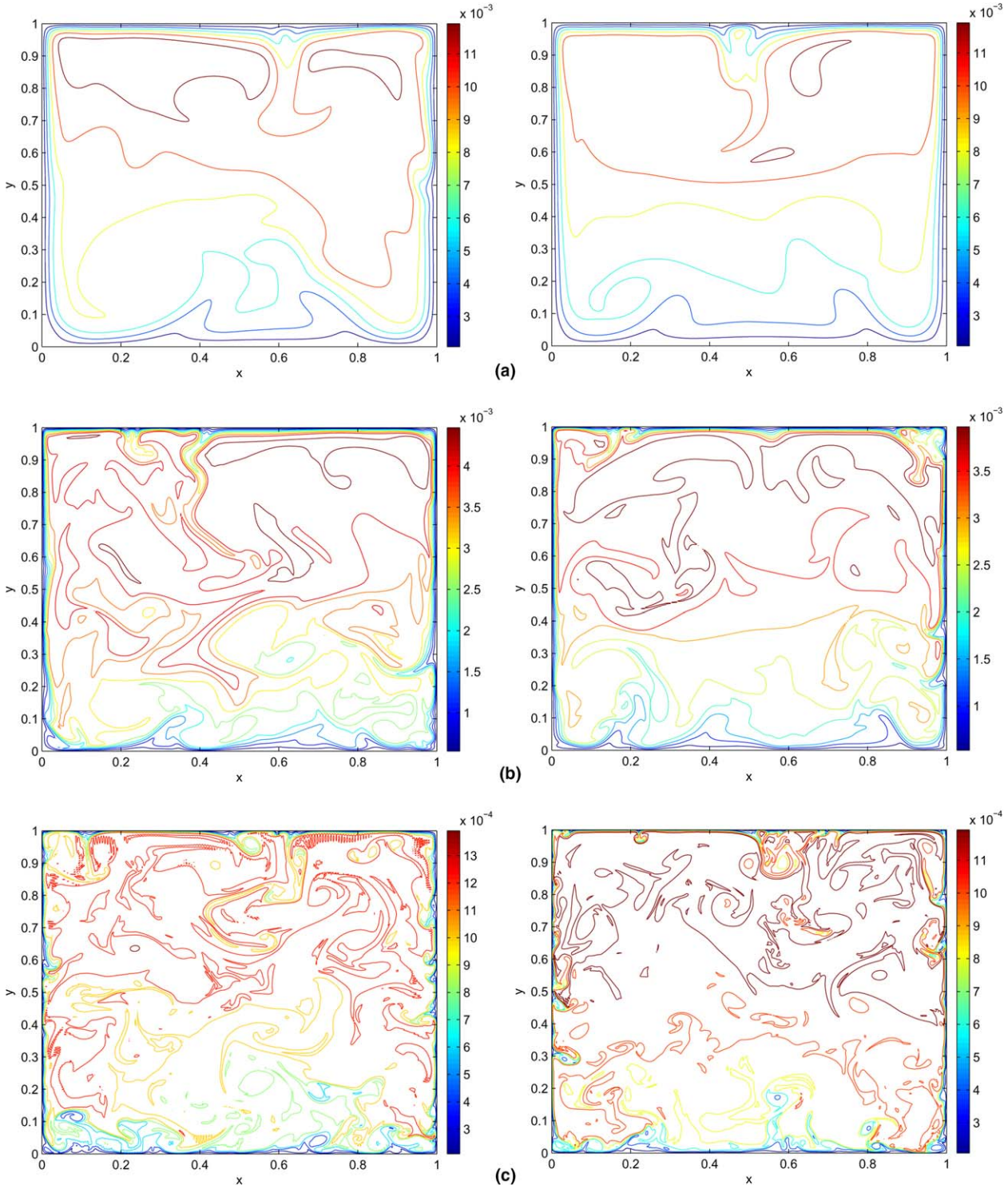

Fig. 2. Isotherms (continued): $Pr = 0.25$ (left) and $Pr = 0.60$ (right). (a) $Ra = 10^9$, (b) $Ra = 10^{11}$, (c) $Ra = 10^{13}$.

with those in Refs. [2,17], which verifies and validates our model. With the increasing of Ra, the effect of the eddy viscosity ν_t becomes significant so that the deviations of Nu between different models on the boundaries set in. On the other hand, it was observed that different Pr will have different effects on the average Nu. A higher Pr enhances heat transfer through the upper and side boundaries, while at the bottom surface of the enclosures a lower Pr enhances heat transfer. Whereas, all the effects are further strengthened at higher $Ra(\geqslant 10^{11})$ for the deviations become increasingly distinctive. Table 1 presents the values of the time-averaged Nu on the upper surface (Nu_{up}) and the relative errors both of our model (TLBGK+LES) and TLBGK model (Ref. [17]) against LES (Ref. [2]). From

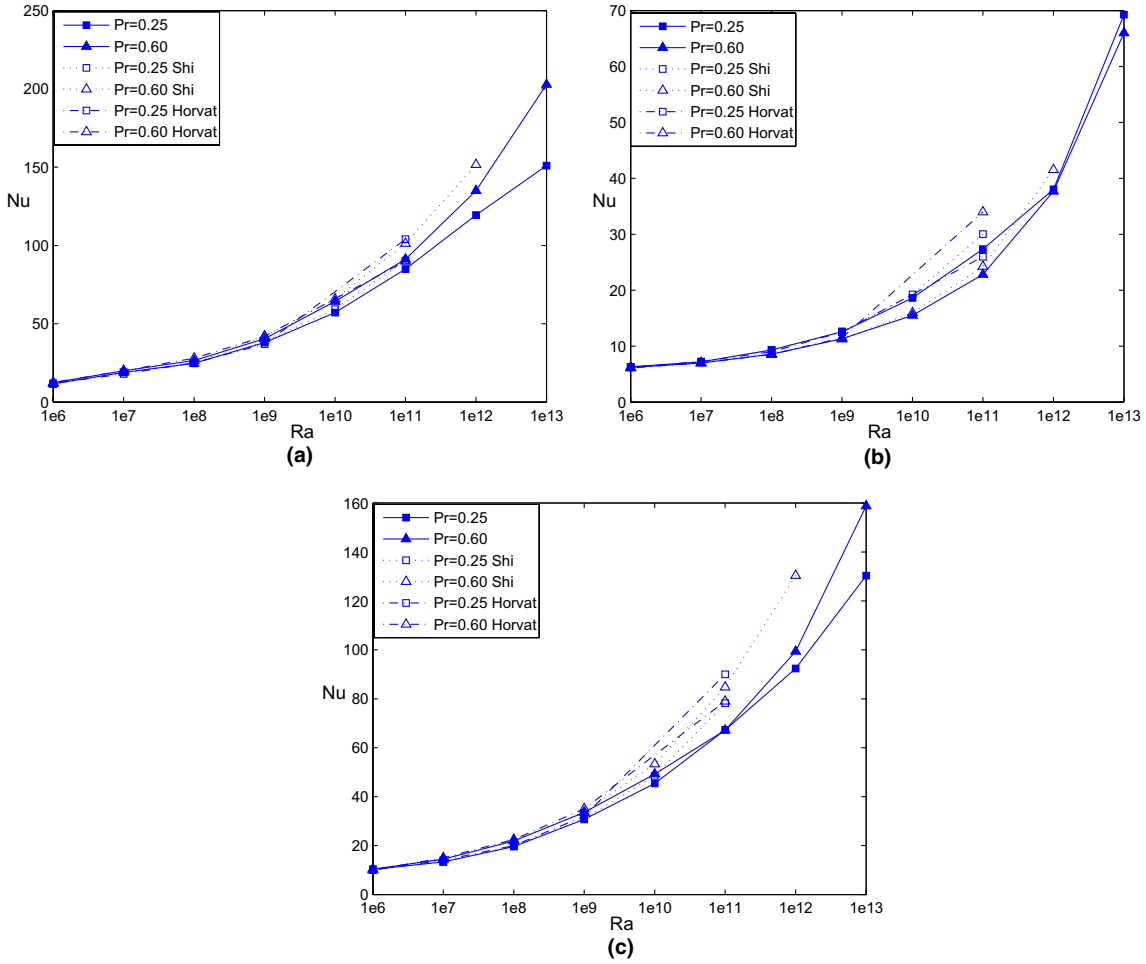

Fig. 3. *Ra* vs. *Nu*: (a) on the upper boundary, (b) on the bottom boundary, (c) on the left boundary.

Table 1
The value of Nu_{up} for different *Ra* and the relative errors

Ra		*Pr* = 0.25	Error	*Pr* = 0.60	Error
10^8	TLBGK + LES	24.6379	−0.0605	26.5248	−0.0588
	TLBGK (Ref. [17])	23.6292	−0.0990	25.1965	−0.1059
	LES (Ref. [2])	26.2258	–	28.18223	–
10^9	TLBGK + LES	38.0221	0.0178	40.4491	−0.0442
	TLBGK (Ref. [17])	33.6443	−0.0994	39.0489	−0.0773
	LES (Ref. [2])	37.3588	–	42.3216	–
10^{11}	TLBGK + LES	84.9468	−0.1436	91.2110	0.0104
	TLBGK (Ref. [17])	84.3260	−0.1499	99.3080	0.1001
	LES (Ref. [2])	99.1952	–	90.2684	–
10^{12}	TLBGK + LES	119.4721	–	134.9829	–
	TLBGK (Ref. [17])	–	–	144.0363	–
10^{13}	TLBGK + LES	125.2459	–	167.7215	–

the table we can also find the values of Nu_{up} increase when *Ra* and *Pr* increase. Contrasting with the TLBGK model, the relative errors of our model against LES are obviously improved.

In Ref. [24], a table of the *Nu*(*Ra*) relationship on the cooled surface in many geometries was presented and one can see that the relationships between Nu_{up} and *Ra* for the upper surface are quite similar to different geometries, which approximately hold $Nu_{up} \approx Ra^{0.20-0.235}$ with *Ra* up to 10^{16}. In our simulations, for *Ra* from 10^9 to 10^{11}, we find $Nu_{up} \approx Ra^{0.1746}$ at $Pr = 0.25$ and $Nu_{up} \approx Ra^{0.1766}$ at $Pr = 0.60$. While *Ra* is between 10^{12} and 10^{13}, we yield $Nu_{up} \approx Ra^{0.1018}$ at $Pr = 0.25$, and $Nu_{up} \approx Ra^{0.1811}$ at $Pr = 0.60$. Hence, even when *Ra* is up to 10^{13}, the exponent can not reach 0.20. There are two possible explanations to the fact: the exponent β will have an increase at higher *Ra*, or the asymptotic state does not exist at all for the turbulent motion at high *Ra* which is too complicated to meet a simple power-law. Further research should be done at higher *Ra* to answer this question.

4. Conclusion

Although the LBGK method has been widely used to simulate natural convection, this is the first time to combine the thermal LBGK model with the LES Smagorinsky model to study high *Ra* thermal convection. Two-dimensional (2D) numerical simulations of natural convection with internal heat generation in a square cavity at *Ra* from 10^6 to 10^{13} with *Pr* 0.25 and 0.60 are performed. Our simulation results agree very well with those published. To our

knowledge, in the previous research work on turbulent natural convection with an internal heat generation, Ra has never exceed 10^{11} with such low $Pr(=0.25)$.

It is well known that the LBGK method has unique advantages, such as the easy arithmetic, easy implementation of boundary conditions and intrinsic parallelism. To simulate the higher Ra flows, the higher resolution is needed, then we will resort to parallel. As the Smagorinsky model does not allow any energy backscatter, other more improved models have been put forward, such as the dynamic Smagorinsky model [28]. Combined these new models to our model, more efficiencies will be gained. Anyway, in possession of the advantages of both the LBGK method and LES, the TLBGK model based on LES is a promising one to simulate turbulent convection at higher Ra.

Our simulation results disclose that at $Ra = 10^{13}$, a global turbulence appears and it can be concluded that with a further increase of Ra, the flow will reach the full turbulent regime. The effect of Pr on the heat transfer still exists at higher Ra and becomes more and more distinctive with increasing Ra.

As a trial, the $Nu(Ra)$ relations have been discussed. The exponent β yielded in our simulation does not reach the reported in existing literatures. As fluid motion becomes turbulent, three-dimensional (3D) effects become dominant. In fact, there are very few events with sustainable 2D turbulence. Therefore, it is reasonable that the results will deviate from a real physical picture. Noted that the TLBGK model can be easily extended to 3D problems, Our further studies will focused on the issue of the existence of an asymptotic regime by the investigations of 3D natural convection problems on even higher Ra flows with different Pr.

Appendix A. Chapman–Enskog expansion

The Chapman–Enskog expansion parameter is the Knudsen number ϵ, defined as

$$\epsilon = \frac{\lambda}{l} \tag{A.1}$$

where λ is the mean free path of the molecules and l is a typical macroscopic length. The derived equations will only be valid if the Knudsen number is small.

Expanding the distribution functions and the time and space derivatives in terms of the Knudsen number

$$\begin{aligned} &\partial_t = \epsilon\partial_{1t} + \epsilon^2\partial_{2t}, \quad \partial_\alpha = \epsilon\partial_{1\alpha}, \\ &f_i = \epsilon f_{1i}, \quad g_i = g_i^{(0)} + \epsilon g_i^{(1)} + \epsilon^2 g_i^{(2)} + \cdots \end{aligned} \tag{A.2}$$

To perform the Chapman–Enskog expansion we must first Taylor expand Eq. (2):

$$\Delta t D_i g_i + \frac{\Delta t^2}{2} D_i^2 g_i = -\frac{1}{\tau}(g_i - g_i^{\mathrm{eq}}) + \Delta t f_i \tag{A.3}$$

where $D_i = \partial_t + \partial_\alpha$. Substituting Eq. (A.2) into Eq. (A.3), we get

$$\begin{aligned} &\epsilon\Delta t D_{1i}(g_i^{(0)} + \epsilon g_i^{(1)}) + \epsilon^2\Delta t\partial_{2t} g_i^{(0)} + \epsilon^2\frac{\Delta t^2}{2} D_{1i}^2 g_i^{(0)} \\ &\quad = -\frac{1}{\tau}(g_i^{(0)} + \epsilon g_i^{(1)} + \epsilon^2 g_i^{(2)} - g_i^{\mathrm{eq}}) + \epsilon\Delta t f_{1i} \end{aligned} \tag{A.4}$$

where $D_{1i} = \partial_{1t} + \partial_{1\alpha}$. And then, we can obtain the following equations in consecutive order of the parameter ϵ:

$$\mathrm{O}(\epsilon^0): \quad g_i^{(0)} = g_i^{\mathrm{eq}} \tag{A.5a}$$

$$\mathrm{O}(\epsilon^1): \quad D_{1i} g_i^{(0)} = -\frac{1}{\tau\Delta t} g_i^{(1)} + f_{1i} \tag{A.5b}$$

$$\mathrm{O}(\epsilon^1): \quad \partial_{2t} g_i^{(0)} + \frac{\Delta t}{2} D_{1i}^2 g_i^{(0)} + D_{1i} g_i^{(1)} = -\frac{1}{\tau\Delta t} g_i^{(2)} \tag{A.5c}$$

Eq. (A.5c) can be simplified by Eq. (A.5b):

$$\partial_{2t} g_i^{(0)} + \left(1 - \frac{1}{2\tau}\right) D_{1i} g_i^{(1)} = -\frac{1}{\tau\Delta t} g_i^{(2)} - \frac{\Delta t}{2} D_{1i} f_{1i} \tag{A.6}$$

The conservation of mass and momentum require that

$$\sum_i g_i^{(k)} = \sum_i c\vec{e}_{i\alpha} g_i^{(k)} = 0, \quad k = 1, 2 \tag{A.7}$$

From the equilibrium distribution function Eq. (3) and the definition of f_i, we can obtain

$$\begin{aligned} &\sum_i g_i^{(0)} = 0, \quad \sum_i c\vec{e}_i g_i^{(0)} = \vec{u}, \\ &\sum_i c^2 \vec{e}_i \vec{e}_i g_i^{(0)} = \vec{u}\vec{u} + pI \end{aligned} \tag{A.8a}$$

$$\sum_i f_i = 0, \quad \sum_i c\vec{e}_i f_i = Pr\theta\frac{\vec{g}}{|\vec{g}|}, \quad \sum_i c^2 \vec{e}_i \vec{e}_i f_i = 0 \tag{A.8b}$$

Taking zeroth-order and first-order moments of Eq. (A.5b), respectively, we can get the following macroscopic equations on the t_1 scale:

$$\partial_{1\alpha} u_\alpha = 0 \tag{A.9a}$$

$$\partial_{t1}\vec{u} + \partial_{1\beta}\pi_{\alpha\beta}^0 = Pr\Theta\frac{\vec{g}}{|\vec{g}|} \tag{A.9b}$$

and where

$$\pi_{\alpha\beta}^0 = \sum_i c^2 \vec{e}_{i\alpha}\vec{e}_{i\beta} g_i^{(0)} = u_\alpha u_\beta + p\delta_{\alpha\beta} \tag{A.10}$$

Taking zeroth-order and first-order moments of Eq. (A.6), respectively, we can get the equations on the t_2 scale:

$$\partial_{t2} u_\alpha + \partial_{1\beta}\pi_{\alpha\beta}^1 = 0 \tag{A.11}$$

Noted that in incompressible flows

$$\mathrm{O}(\delta p) = \mathrm{O}(\delta\rho) = \mathrm{O}(Ma^2) \tag{A.12a}$$

$$\mathrm{O}(u) = \mathrm{O}(Ma) \tag{A.12b}$$

in the limit $Ma \to 0$, where δp and $\delta\rho$ are the pressure and density fluctuations, respectively. And then, with the aims of Eq. (A.5b) and Eq. (A.10), the stress tensor $\pi_{\alpha\beta}^1$ is given by

$$\begin{aligned}\pi^1_{\alpha\beta} &= \left(1-\frac{1}{2\tau}\right)\sum_i c^2\vec{e}_{i\alpha}\vec{e}_{i\beta}g_i^{(1)}\\ &= \left(1-\frac{1}{2\tau}\right)\sum_i c^2\vec{e}_{i\alpha}\vec{e}_{i\beta}\tau\Delta t(f_i - D_{1i}g_i^{(0)})\\ &= -\left(\tau-\frac{1}{2}\right)\Delta t\sum_i c^2\vec{e}_{i\alpha}\vec{e}_{i\beta}D_{1i}g_i^{(0)}\\ &= -\frac{c^2}{3}\left(\tau-\frac{1}{2}\right)\Delta t(\partial_{1\alpha}u_\beta+\partial_{1\beta}u_\alpha)+\mathrm{O}(Ma^2)\\ &= -\nu(\partial_{1\alpha}u_\beta+\partial_{1\beta}u_\alpha)+\mathrm{O}(Ma^2)\end{aligned} \tag{A.13}$$

In the above equation, the terms of order $\mathrm{O}(u^3)$ or higher have been neglected. Combining the results on the t_1 and t_2 time scales, Eqs. (A9) and (A.10) together with Eq. (A.11) and (A.13), we now obtain the final macroscopic Eqs. (1a) and (1b). From Eq. (A.13) , the strain rate tense $S_{\alpha\beta}$ is given by

$$\begin{aligned}S_{\alpha\beta} &= (\partial_\alpha\bar{u}_\beta+\partial_\beta\bar{u}_\alpha)/2 = \epsilon(\partial_{1\alpha}\bar{u}_\beta+\partial_{1\beta}\bar{u}_\alpha)/2\\ &\approx \frac{3\epsilon}{2\tau\Delta t}\sum_i\vec{e}_{i\alpha}\vec{e}_{i\beta}g_i^{(1)}\\ &= \frac{3\epsilon}{2\tau\Delta t}\sum_i\vec{e}_{i\alpha}\vec{e}_{i\beta}(g_i-g_i^{(0)})/\epsilon\\ &= \frac{3}{2\tau\Delta t}\sum_i\vec{e}_{i\alpha}\vec{e}_{i\beta}(g_i-g_i^{(0)})\end{aligned} \tag{A.14}$$

References

[1] E.D. Siggia, High Rayleigh number convection, Annu. Rev. Fluid Mech. 26 (1994) 137–168.

[2] A. Horvat, I. Kljenak, J. Marn, Two-dimensional large-eddy simulation of turbulent natural convection due to internal heat generation, Int. J. Heat and Mass transfer 44 (2001) 3985–3995.

[3] N. Cantin, A.P. Vincent, D.A. Yuen, Large eddy simulations of thermal convection at high Rayleigh number, Geophys. J. Int. 140 (2000) 163–174.

[4] J.J. Niemela, L. Skrbek, K.R. Sreenivasan, R.J. Donnelly, Turbulent convection at very high Rayleigh numbers, Nature 404 (2002) 837–840.

[5] A.P. Vincent, D.A. Yuen, Transition to turbulent thermal convection beyond $Ra = 10^{10}$ detected in numerical simulations, Phys. Rev. E 61 (2000) 5241–5246.

[6] J. Smagorinsky, General circulation experiments with the primitive equations, Part I: the basic experiments, Mon. Weather Rev. 91 (1963) 99–164.

[7] A. Horvat, Modeling of turbulent natural convection in a fluid with internal heat generation with the large-eddy simulation method, Ph.D. Thesis, Faculty of Mathematics and Physics, University of Ljubljana, Ljubljana, Slovenia, 2001.

[8] S. Chen, G.D. Doolen, Lattice Boltzmann method for fluid flows, Annu. Rev. Fluid Mech. 30 (1998) 329–364.

[9] L.-S. Luo, The lattice-gas and lattice Boltzmann methods: past, present, and future, in: Proc. Int. Conf. Applied CFD, Beijing, 2000, pp. 52–837.

[10] X. Shan, Simulation of Rayleigh–Bénard convection using a lattice Boltzmann method, Phys. Rev. E 55 (1997) 2780–2788.

[11] X. He, S. Chen, G.D. Doolen, A novel thermal model for the lattice Boltzmann method in incompressible limit, J. Comput. Phys. 146 (1998) 282–300.

[12] F.J. Alexander, S. Chen, J.D. Sterling, Lattice Boltzmann thermohydrodynamics, Phys. Rev. E 47 (1993) 2249–2252.

[13] G.R. McNamara, A.L. Garcia, B.J. Alder, Stabilization of thermal lattice Boltzmann models, J. Stat. Phys. 81 (1995) 395–408.

[14] Z.-L. Guo, B.-C. Shi, C.-G. Zheng, A coupled lattice BGK model for the Bouessinesq equation, Int. J. Num. Meth. Fluids 39 (2002) 325–342.

[15] A. DÓrazio, S. Succi, C. Arrighetti, Lattice Boltzmann simulation of open flows with heat transfer, Phys. Fluids 15 (9) (2003) 2778–2781.

[16] A. DÓrazio, M. Corcione, G.P. Celata, Application to natural convection enclose flows of a lattice Boltzmann BGK model coupled with a general purpose thermal boundary condition, Int. J. Thermal Sci. 43 (2004) 531–630.

[17] B.-C. Shi, Z.-L. Guo, Thermal lattice BGK simulation of turbulent natural convection due to internal heat generation, Int. J. Mod. Phys. B 9 (2002) 48–51.

[18] S. Hou, J. Sterling, S. Chen, G.D. Doolen, A lattice Boltzmann subgrid model for high Reynolds number flows, Fields Inst. Comm. 6 (1996) 151–166.

[19] C.M. Teixeira, Incorporation turbulence models into the lattice-Boltzmann method, Int. J. Mod. Phys. C 9 (1998) 1159–1175.

[20] M. Krafczyk, J. Tölke, L.-S. Luo, Large-eddy simulations with a multiple-relaxation-time LBE model, Int. J. Mod. Phys. B 17 (2003) 33–39.

[21] X.Z. Wu, A. Libchaber, Scaling relations in thermal turbulence: the aspect ratio dependence, Phys. Rev. A 45 (1992) 842–845.

[22] S. Grossmann, D. Lohse, Scaling in thermal convection: a unifying theory, J. Fluid Mech. 407 (2000) 27–56.

[23] R.H. Kraichnan, Turbulent thermal convection at arbitrary Prandtl number, Phys. Fluids 5 (1962) 1374–1389.

[24] R.R. Nourgaliev, T.N. Dinh, B.R. Sehgal, Effect of fluid Prandtl number on heat transfer characteristics in internally heated liquid pools with Rayleigh numbers up to 10^{12}, Nuc. Eng. Des. 169 (1997) 165–184.

[25] A. Horvat, Modeling of natural convection phenomena in nuclear reactor core melt, M.Sc. Thesis, Faculty of Mathematics and Physics, University of Ljubljana, Ljubljana, Slovenia, 1998. Available from: <http://www2.ijs.si/ahorvat>.

[26] Z.-L. Guo, B.-C. Shiand, N.-C. Wang, Lattice BGK model for incompressible Navier–Stokes equation, J. Comput. Phys. 165 (2000) 288–306.

[27] Y. Qian, D. d'Humiéres, P. Lallemand, Lattice BGK models for Navier–Stokes equation, Europhys. Lett. 17 (1992) 479–484.

[28] M. Germano, U. Piomelli, P. Moin, W.H. Cabot, A dynamic subgrid-scale eddy viscosity model, Phys. Fluids A 4 (1992) 633–635.